IIM

CrossMark

TECHNICAL PAPER

In Situ Observation of the Lengthening Rate of Bainite Sheaves During Continuous Cooling Process in a Fe–C–Mn–Si Superbainitic Steel

Junyu Tian[1,2] · Guang Xu[1] · Li Wang[2] · Mingxing Zhou[1] · Haijiang Hu[1]

Abstract The evolution of lengthening rate of bainite sheaves during continuous cooling process in a Fe–C–Mn–Si superbainitic steel was investigated by in situ observation on high-temperature laser scanning confocal microscope. The lengthening rates of bainite sheaves in three temperature ranges were calculated. The results indicate that the lengthening rate of bainite sheaves continuously decreases with the decrease of temperature during continuous cooling process. The lengthening rate of bainite sheaf depends on undercooling, transformation temperature, the diffusion of carbon atoms and the carbon content in parent austenite etc. The lengthening rate at high temperature is large due to the favorable carbon diffusion, smaller carbon content and less plastic deformation in untransformed austenite. Additionally, the microstructures after different isothermal holding temperatures were analyzed, indicating that the larger lengthening rate of bainite sheaves due to the high isothermal transformation temperature does not mean more amount of bainite transformation. Lower bainitic transformation temperature results in more and finer bainite plates.

1 Introduction

Since Bain first reported bainite in 1930s [1–3], bainitic transformation has been a hot topic [4–6]. Bainite is an important product of austenite decomposition. Bainitic transformation occurs in the temperature range between the upper temperature transformations, such as pearlite or ferrite [7], classically described as diffusive, and the lower temperature transformations traditionally described as displacive such as the martensitic transformations [8].

Metallography and dilatometry are popular methods for the investigation of bainitic transformation. However, the conventional metallographic investigation can only watch the bainite morphology after transformation for a certain time. The continuous lengthening of bainite plates cannot be directly observed. In recent years, high-temperature laser scanning confocal microscope (LSCM) has been used as a practicable approach in some studies to directly observe bainite transformation [9–15]. The advantage of this approach is that, the dynamic phase transformation process at any temperature and time can be observed in real time. Xu et al. [9] analyzed qualitatively the evolution of bainite ferrite during the isothermal phase transition using LSCM for in situ observation at different austenization temperatures. LSCM was also used by Kolmskog et al. [10]

✉ Guang Xu
xuguang@wust.edu.cn

Junyu Tian
13164178028@163.com

Li Wang
lwang@baosteel.com

Mingxing Zhou
kdmingxing@163.com

Haijiang Hu
hhjsunny@sina.com

1 The State Key Laboratory of Refractories and Metallurgy, Key Laboratory for Ferrous Metallurgy and Resources Utilization of Ministry of Education, Wuhan University of Science and Technology, Wuhan 430081, China

2 State Key Laboratory of Development and Application Technology of Automotive Steels (Baosteel Group), Shanghai 201900, China

to directly observe bainite isothermal formation below the martensite start temperature (M_S). In addition, Hu et al. [14] investigated the growth rate of bainite plates on the isothermal transformation process in superbainitic steel using LSCM. The dynamic observations of isothermal bainite transformation in a Fe–C–Mn–Si superbainitic steel were conducted using LSCM by Hu et al. [15].

However, previous studies on bainite transformation by in situ observation focused on the process of isothermal transformation [9–11, 14, 15]. The evolution of bainite lengthening rate during continuous cooling process has rarely been reported. In most industrial cases, bainite transformation normally occurs during continuous cooling, so the investigation of bainite lengthening during continuous cooling is necessary. During continuous cooling process, the chemical driving force for nucleation and growth increases, whereas the diffusion ability of carbon atoms decreases with the decrease of temperature. Besides, the carbon content in parent austenite affects the lengthening of subsequent bainite plates. Therefore, the lengthening of bainite during continuous cooling process is affected by multiple factors. It is important to investigate the lengthening of bainite during continuous cooling process and provide the theoretical reference for the control of bainite transformation in industrial production scenario.

In the present study, the lengthening of bainite sheaves during continuous cooling process was dynamically observed by LSCM. The lengthening rates of bainite sheaves nucleating at grain boundaries and within grains were measured, respectively, in different temperature ranges. The evolution of lengthening rate of bainite sheaves during continuous cooling was analyzed.

2 Materials and Methods

A superbainitic steel with the chemical composition of 0.40C, 2.81Mn, 2.02Si, balance Fe (wt%) was used in the present study. The material was refined in a vacuum induction furnace and cast into a small ingot followed by rolling to a 10 mm thick flat. Samples for LSCM were machined to a cylinder of 6 mm diameter and 4 mm height. The dimension of the samples could avoid temperature gradient along the thickness of the sample. The top and bottom surfaces of samples were polished conventionally to keep the measurement face level and minimize the effect of surface roughness. The investigations were conducted using a VL2000DX-SVF17SP LSCM. The specimen chamber was initially evacuated to 6×10^{-3} Pa before heating and argon was used to protect specimens from surface oxidation. The specimens were heated at a rate of 5 °C/s to the austenization temperature (i.e., 1100 °C) and held for 15 min. Then the specimens were

cooled to 330 and 430 °C at a rate of 5 °C/s, respectively, and isothermally treated for 60 min for bainitic transformation followed by final air cooling to room temperature. Meanwhile, in order to analyze the bainite transformation, thermal simulation experiments were conducted by the same test procedures on a Gleeble-3500 simulator. The cylindrical samples with a diameter of 8 mm and a length of 12 mm were used. The dilatations along the radial direction were measured during the entire experimental process. For the tested steel, the bainite starting temperature (B_S) and the martensite starting temperature (M_S) were calculated for 536 and 258 °C according to the empirical Eqs. (1) and (2) [16, 17].

$$B_S = 745 - 110C - 59Mn - 39Ni - 68Cr - 106Mo + 17MnNi + 6Cr^2 + 29Mo^2; \qquad (1)$$

$$M_S = 496.1(1 - 0.620C)(1 - 0.092Mn)(1 - 0.033Si)$$
$$(1 - 0.045Ni)(1 - 0.070Cr)(1 - 0.029Mo)$$
$$(1 - 0.013W)(1 + 0.120Co). \qquad (2)$$

The calculated results were consistent with the temperature–time-transformation (TTT) curve shown in Fig. 1. The TTT curve was plotted by the software MUCG 83 developed by Bhadeshia at Cambridge University [5]. Thus, the isothermal transformation temperature was designed to be 330 and 430 °C. The purpose of using two isothermal temperatures for bainitic transformation was to investigate the relationship between the lengthening rate and bainite amount. In order to expediently contract the lengthening rate of bainite sheaves, the cooling process of a type of thermal treatment from B_S to lower isothermal transformation temperature (i.e., 330 °C) was divided into three temperature ranges. They were high temperature range (500–550 °C, HTR), medium temperature range
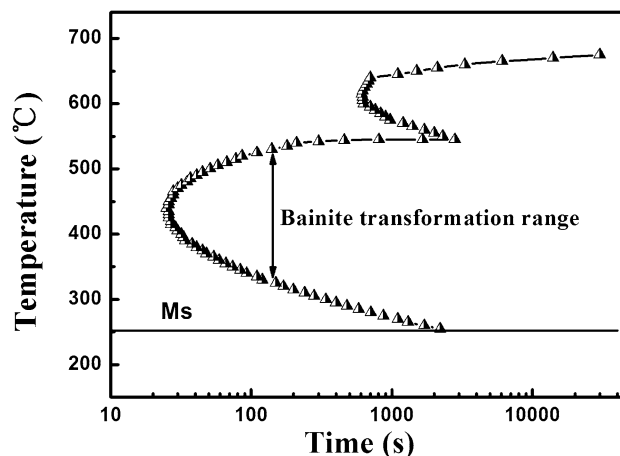
Fig. 1 The time–temperature-transformation (TTT) *curve* for the tested steel

(430–500 °C, MTR) and low temperature range (330–430 °C, LTR), respectively.

The LSCM images were recorded continuously at 5 frames per second during the whole treatment process. A video showing bainite transition process was simultaneously obtained. The principle for in situ observation of bainite nucleation and growth was the relief phenomenon occurring in phase transition. Ko and Cottrell [18] first observed the relief phenomenon of bainitic transformation in 1952. The final microstructure and grain size were observed on a Nova 400 Nano field emission scanning electron microscope (FE-SEM) operated at an accelerating voltage of 20 kV and Zeiss optical microscope (OM). Furthermore, the microhardness of different phases was measured on HV-1000 metallographic microhardness tester.

3 Results and Discussions

3.1 Lengthening Rate of Bainite Sheaves

It is reported that bainite nuclei can initiate at austenite grain boundaries and within austenite grains [14, 15]. After nucleation, the lengthening of bainite ferrite sheaves can be directly monitored using in situ observation by LSCM. Figure 2 shows the dilatation versus temperature during the entire treatments for the sample transformed at 430 °C. It can be observed that the phase transition occurs when the temperature decreases to the point M (about 534 °C) during the continuous cooling process. It demonstrates that phase transformation occurs in the range of 500–550 °C. Combined with the TTT curve (Fig. 1) and the calculated result of B_S (536 °C), it is reasonable to infer that this transformation is bainite transition.
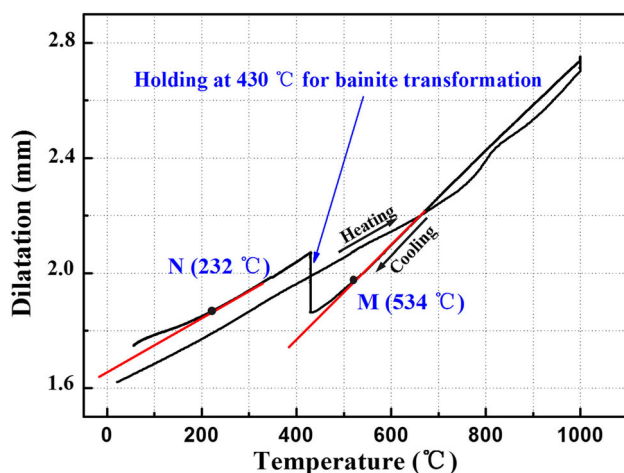
Fig. 2 The dilatation versus temperature for the sample transformed at 430 °C during the entire heat treatments

Figures 3, 4 present the average lengthening rate of bainite in HTR (500–550 °C). The lengthening process of bainite sheaf nucleated within a grain is presented in Fig. 3, while Fig. 4 illustrates the lengthening of bainite sheaf at an austenite grain boundary. The lengthening of bainite sheaves is related to the crystallography with parent matrix, and the lengthening of the sheaves may depend on orientation relationship of the sheaves with matrix in austenite [19]. In this study, the average lengthening rate is focused and crystallography effect has not been considered. The lengthening rate is determined by the slope of the length-to-time plot. Figure 3a shows the length of a bainite sheaf at 1439.65 s, and Fig. 3b, c indicate it's lengthening over time. According to the lengths of the bainite sheaf at various times, the lengthening curve of the bainite sheaf nucleated in austenite grains is plotted in Fig. 3d. Similarly, the lengthening rates of bainite sheaves nucleated at austenite grain boundaries in HTR are also obtained as shown in Fig. 4d.

The lengthening rates are obtained by the slope of the length-to-time plot (Figs. 3d, 4d). It can be calculated that the lengthening rates within austenite grains and at grain boundaries are 16.15 and 21.48 μm/s in HTR (500–550 °C), respectively. Similarly, the lengthening processes in MTR (430–500 °C) and LTR (330–430 °C) are illustrated in Figs. 5, 6, 7 and 8. Figure 5 shows the LSCM micrographs of a bainite sheaf nucleated within an austenite grain in MTR at a lengthening rate of 10.71 μm/s and at a grain boundary with a rate of 12.57 μm/s (Fig. 6). Figures 7, 8 present the lengthening processes of bainite sheaves in LTR at the lengthening rate of 4.57 and 4.16 μm/s, within a grain and at a grain boundary, respectively.

In summary, the curves of the lengthening rate with temperature are presented in Fig. 9. It can be observed that the lengthening rate of bainite sheaves decreases with the decrease of temperature. According to the results in Fig. 9, the empirical equation for the prediction of the lengthening rate of bainte sheaf at different temperatures is proposed as follows:

$$v = a_0 T + a_1 \tag{3}$$

where, v represents the lengthening rate of bainite sheaf, T the temperature, a_0 and a_1 are the related coefficients. The values of a_0 and a_1 are 0.117 μm/(s °C) and −42.89 μm/s within grain, whereas they are 0.143 μm/(s °C) and −54.32 μm/s at grain boundary, respectively.

A viewpoint acknowledged by many scholars is that, the lengthening process of bainite sheaves is the accumulation of nucleation and growth of many sub-units. A sub-unit nucleates at austenite grain boundary and lengthens until its growth is arrested by plastic deformation within the austenite. New sub-units then nucleate at its tip, and the sheaf structure developed as this process continues as
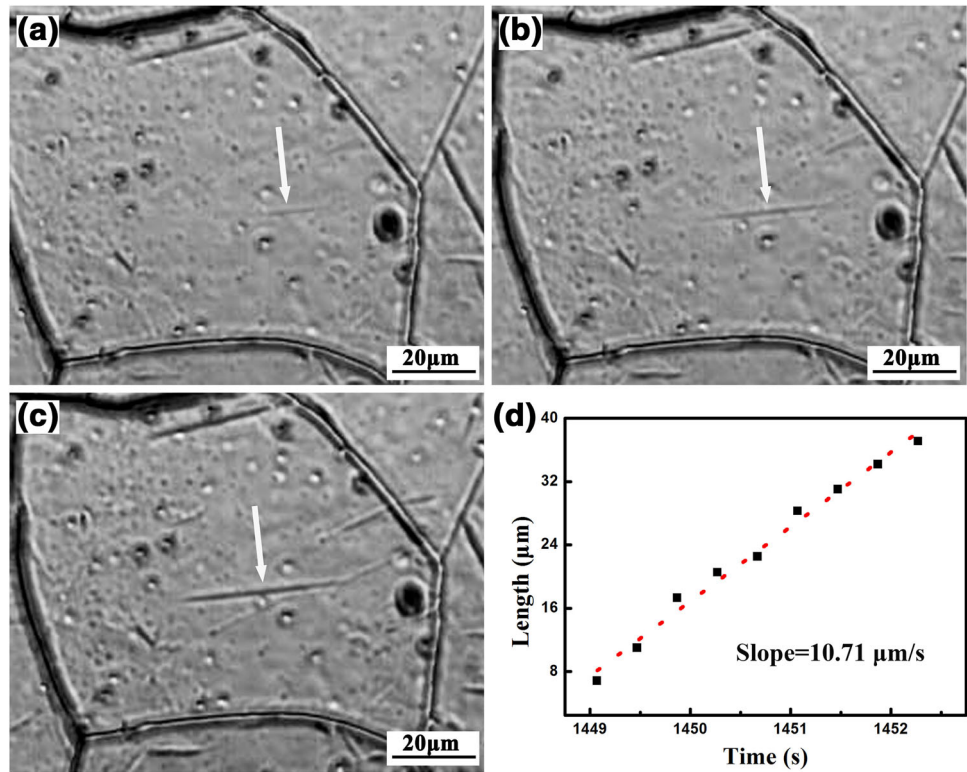
Fig. 3 Micrographs of the lengthening of a bainite sheaf nucleated within grain in 500–550 °C: **a** 1439.65 s, 507.2 °C; **b** 1440.87 s, 501.8 °C; **c** 1441.27 s, 500.6 °C and **d** length-time plot
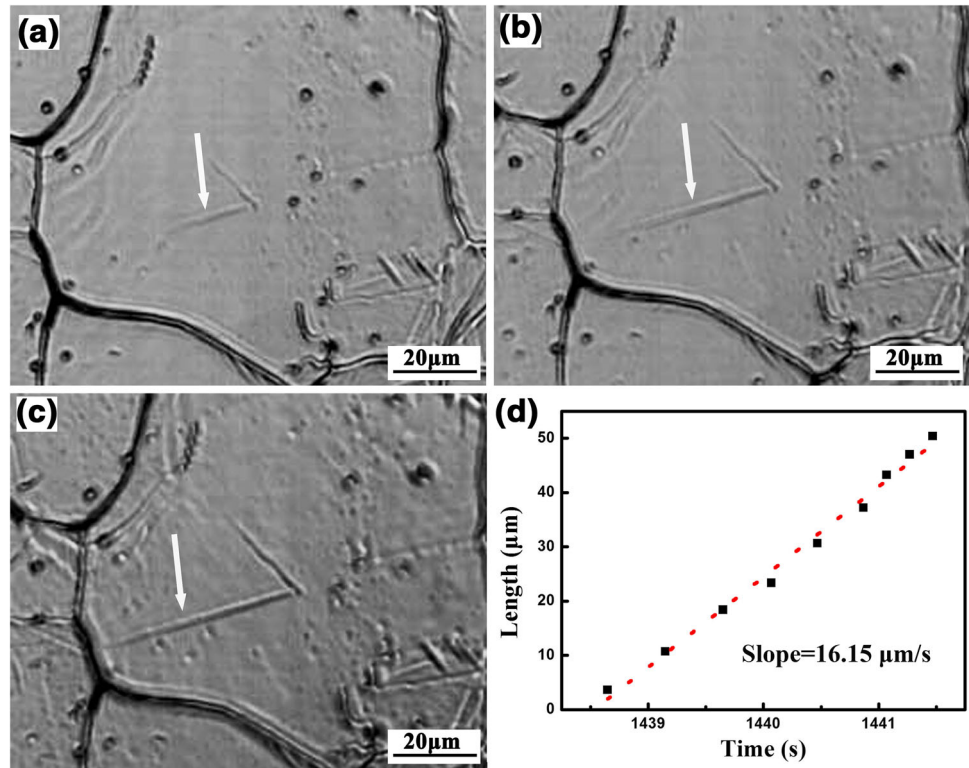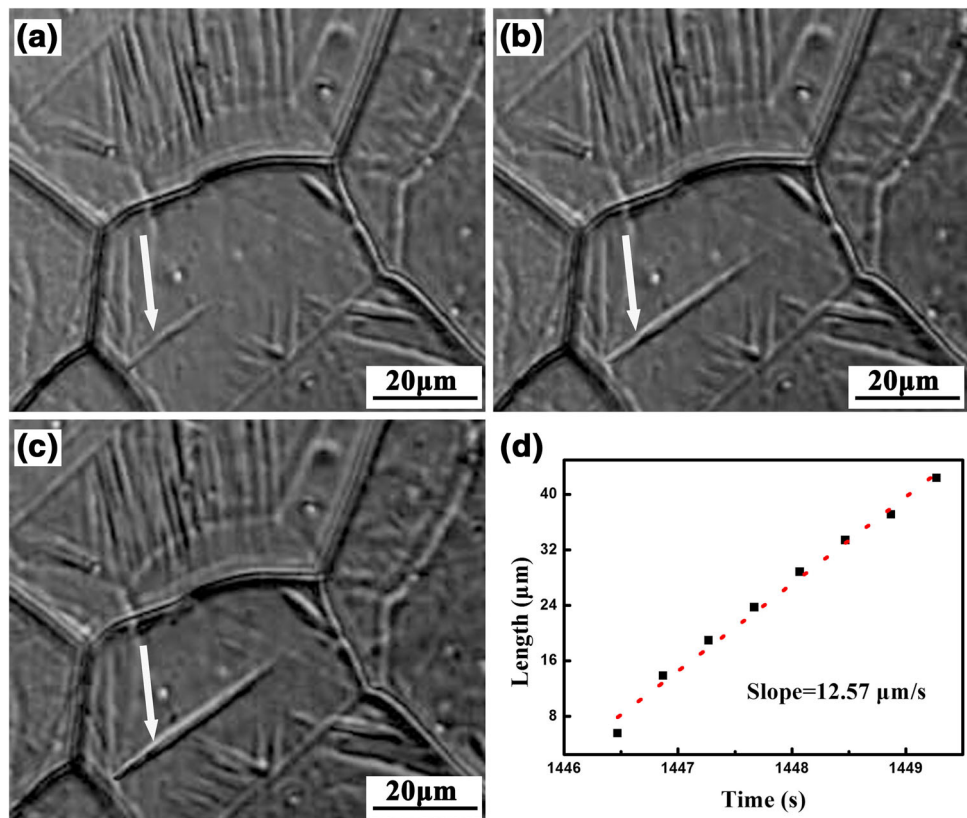

Fig. 4 Micrographs of the lengthening of a bainite sheaf nucleated at grain boundary in 500–550 °C: **a** 1434.15 s, 533.7 °C; **b** 1434.65 s, 530.7 °C; **c** 1435.15 s, 529.3 °C and **d** length-time plot
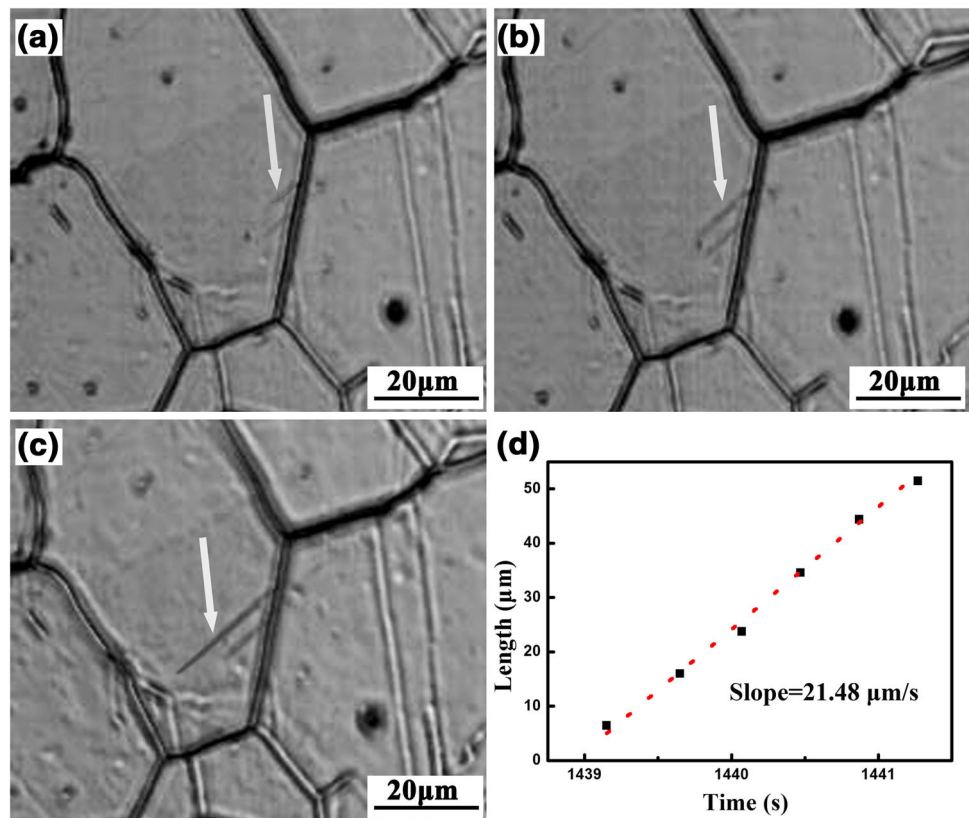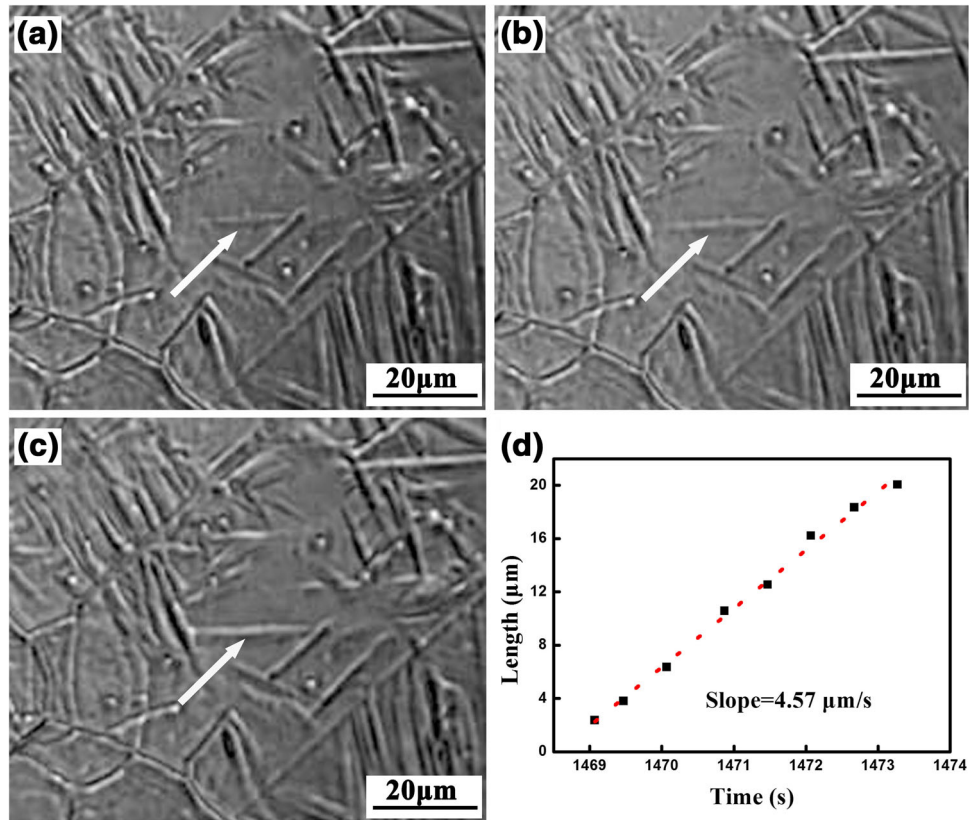
Fig. 5 Micrographs of the lengthening of a bainite sheaf nucleated within grain in 430–500 °C: **a** 1449.67 s, 466.5 °C; **b** 1451.07 s, 461.1 °C; **c** 1454.07 s, 453.2 °C and **d** length-time plot


Fig. 6 Micrographs of the lengthening of a bainite sheaf nucleated at grain boundary in 430–500 °C: **a** 1447.47 s, 474.2 °C; **b** 1449.07 s, 468.5 °C; **c** 1452.87 s, 456.0 °C and **d** length-time plot

Fig. 7 Micrographs of the lengthening of a bainite sheaf nucleated within grain in 330–430 °C: **a** 1471.87 s, 413.0 °C; **b** 1473.27 s, 408.0 °C; **c** 1478.07 s, 393.7 °C and **d** length-time plot

Fig. 8 Micrographs of the lengthening of a bainite sheaf nucleated at grain boundary in 330–430 °C: **a** 1467.87 s, 424.3 °C; **b** 1471.47 s, 414.0 °C; **c** 1478.87 s, 391.0 °C and **d** length-time plot
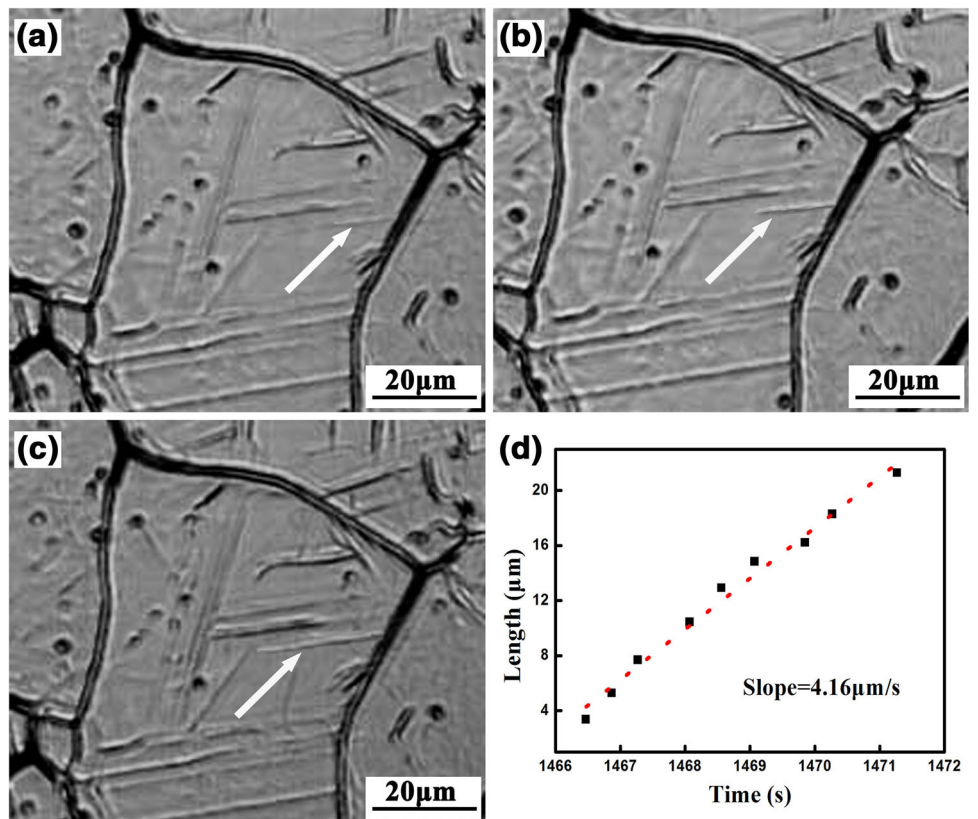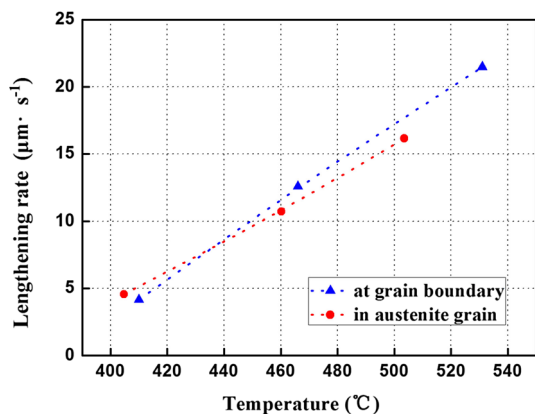
Fig. 9 The lengthening rates of bainite sheaves during continuous cooling process
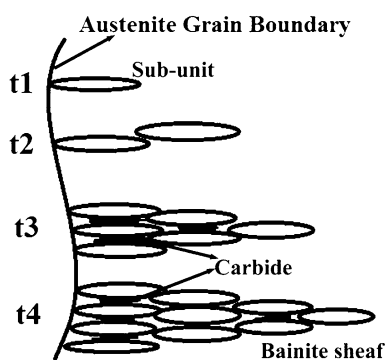

Fig. 10 The schematic diagram of lengthening process of bainite sheaf [20]

shown in Fig. 10. Bainite transformation consists of nucleation and growth. Compared to nucleation, the growth of bainite sub-unit is much faster [20]. Therefore, the nucleation rate has a crucial role in the lengthening rate of bainite sheaf.

It is well known that the lengthening rate of bainite sheaf depends on undercooling, transformation temperature, the diffusion of carbon atoms and the carbon content in parent austenite etc. It has been proved in Ref. [21] that the nucleation rate of bainitic ferrite decreases with decreasing temperature. Kang et al. [22] studied the bainite growth during bainite transformation, and they reported that the lengthening rate is well consistent with values calculated by the models of carbon diffusion control [23, 24]. Additionally, Christian [25] stated the relationship between temperature and the nucleation rate, and indicated that the temperature dependence is controlled only by the carbon diffusion and not by the driving force. Nucleation rate (N_α) is given by Luzginova et al. [26] as in Eq. (4). Additionally, the relationship between the ability of carbon diffusion and temperature is given in Eq. (5) [27]. According to Eqs. (4, 5), the relationship between Nucleation rate and carbon diffusion can be deduced as Eq. (6).

$$N_\alpha = N_{0\alpha} \frac{k_B T}{h} \exp\left(-\frac{Q_i}{RT}\right) \qquad (4)$$

$$D = D_0 \exp\left(-\frac{Q_i}{RT}\right) \qquad (5)$$

$$N_\alpha = N_{0\alpha} \frac{k_B T}{h} \frac{D}{D_0} \qquad (6)$$

where, $N_{0\alpha}$ is the initial site density, R the gas constant, T the temperature, h the Planck constant and k_B is the Boltzmann constant. Q_i is the activation energy representing the barrier to transfer atoms across the interface. D and D_0 are the diffusion coefficient and the diffusion constant of carbon in austenite, respectively. The values of R, D_0 and Q_i are respectively 8.31 J/(mol·K), 0.23 cm^2/s and 138 kJ/mol in austenite [27]. From Eq. (5), the values of D from 330 to 550 °C can be calculated and the calculated results are shown in Fig. 11a. It indicates that the value of D obviously decreases with the temperature. Eq. (6), shows that the nucleation rate largely depends on D and decreases with the decrease of temperature. Additionally, Fig. 11b presents the lengthening rate of bainite sheaf as a function of D of carbon. The empirical Eq. (7) can be obtained from the curve in Fig. 11b, and it can be used to predict the relationship between the lengthening rate of bainte sheaf and D of carbon at different temperatures.

$$v = b_{0*} (lgD)^2 + b_1 * lgD + b_2 \qquad (7)$$

where, v represents the lengthening rate of bainite sheaf, D the diffusion coefficient of carbon, b_0, b_1 and b_2 are the related coefficients. The values of b_0, b_1 and b_2 are 0.3118, 13.7228 and 151.60876 within grain, whereas they are 0.18078, 10.18697 and 129.78633 at grain boundary, respectively.

When bainitic transformation occurs in HTR, the ability of carbon diffusion and the sub-unit nucleation rate is high, which leads to faster lengthening of bainite sheaves. In MTR and LTR, although the undercooling is large due to the lower temperature, the speed of carbon atom diffusion and the nucleation rate decreases. It has been shown in [28] that carbon diffusion is the main controlling parameter for the nucleation rate of bainitic ferrite. Moreover, bainite transformation continuously occurs during the cooling process. The extra carbon diffuses into the adjacent austenitic area during the process of bainite transformation, resulting in the enrichment of carbon in untransformed austenite. The enrichment of carbon stabilizes austenite and makes it difficult for further decomposition of austenite. Additionally, bainite transformation is accompanied by plastic accommodation in austenite, leading to the stabilization of austenite [29]. Therefore, the lengthening rate of bainite sheaves decreases with the decrease of temperature.

Fig. 11 The relationship between: **a** the diffusion coefficient and the temperature, **b** the lengthening rate and the diffusion coefficient
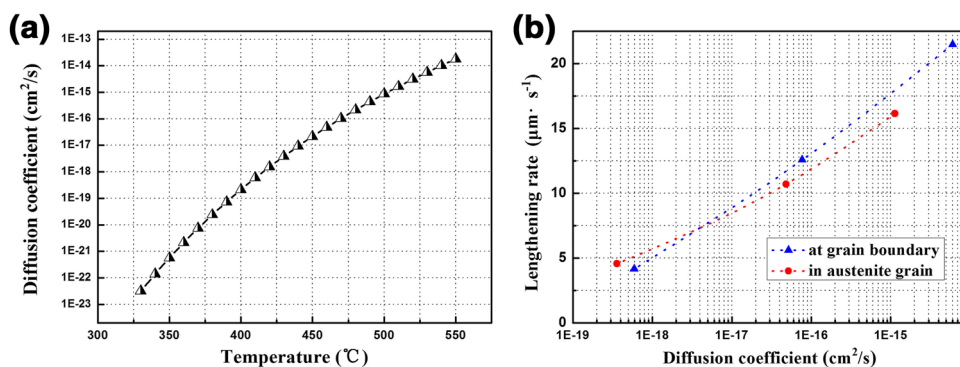
Fig. 12 Comparison of the microstructures after isothermal transformation at 330 and 430 °C: **a**, **c** 330 °C; **b**, **d** 430 °C
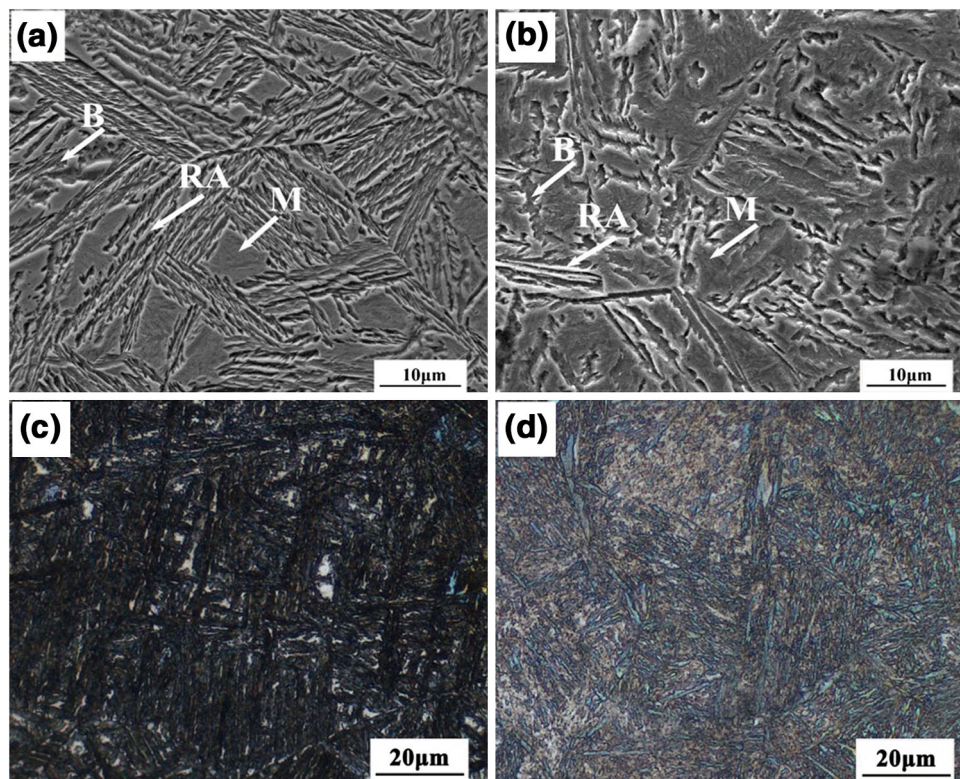
From Fig. 9, it can also be observed that the lengthening rate of bainite sheaves nucleated at grain boundaries is faster than that within grains in HTR and MTR. It is consistent with the result in Ref. [14]. Irregular atomic arrangements and lattice distortions at grain boundaries lead to high energy, which contributes to bainite nucleation. Moreover, the higher diffusion speed of atoms at grain boundaries due to the presence of more defects such as dislocations and vacancies increases the nucleation rate. The nucleation and growth of new nuclei at grain boundaries can consume the grain energy in a spontaneous process. Therefore, the lengthening rate at grain boundary is larger than that initiated in grain. However, Hu et al. [14] only studied the relationship of the lengthening rate between at grain boundary and within grain during the

process of isothermal transformation. The evolution of the lengthening rate during continuous cooling process is investigated in the present study. It can also be observed from Fig. 9 that in LTR, the lengthening rate of bainite sheaf nucleated at grain boundary equals basically that initiating within grain. The reason is that, more bainite forms at grain boundary due to easy nucleation and more plastic deformation appears, resulting in more stabilization of austenite. Therefore, the lengthening rate of bainite sheaves at grain boundary slows down.

3.2 Microstructures

The SEM and OM micrographs after isothermal transformation at 330 and 430 °C are shown in Fig. 12. The

Fig. 13 a Dilatation curves and **b** bainite transformation volume fraction with time during isothermal holding at 330 and 430 °C
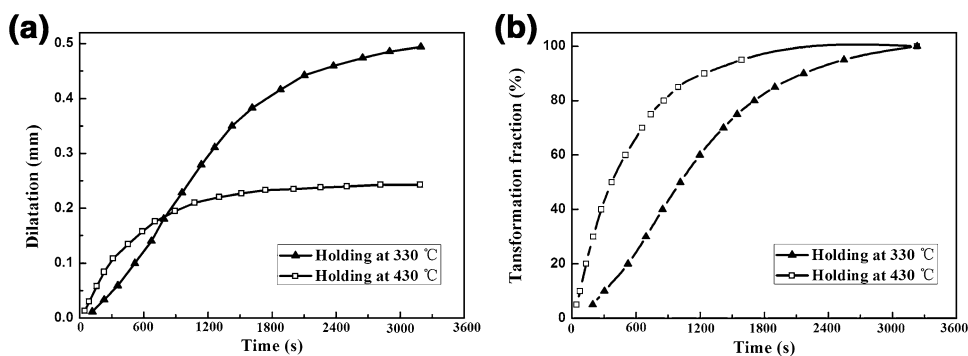
microstructures are useful to analyze the relationship between the lengthening rate and bainite amount. The microstructure consists of bainite (B), martensite (M) and retained austenite (RA). It can be observed from Fig. 12 that the bainite plate in the sample isothermally transformed at 330 °C are more and finer compared to the samples transformed at 430 °C. In addition, the microhardnesses of two samples have been measured, which are 455 and 489 HV, respectively.

As discussed in previous section, the lengthening rate decreases with the decrease of temperature, indicating that the lengthening rate of bainie sheaf at 430 °C is higher than that at 330 °C. However, the bainite amount transformed at 430 °C is less than that transformed at 330 °C. The dilatation results in Fig. 13 demonstrate the same conclusions. Figure 13a presents the dilatations as a function of holding time during the isothermal transformation process, while Fig. 13b shows the relationship of volume fraction of bainite with time during isothermal transformation process. The calculated M_S is 258 °C for the tested steel, indicating that no martensite forms during the isothermal transformation process at 330 and 430 °C. Additionally, the point N (about 232 °C, Fig. 2) represents the measured M_S. Therefore, martensite in Fig. 12 forms during the cooling after bainite isothermal transformation.

As stated above, it demonstrates that the higher lengthening rate of bainite sheaves does not mean more amount of final bainite. It can be explained by the T_0-theory [30–32]. Figure 14 shows the schematic illustration of T_0 and T'_0 curve. T_0 curve is the locus of all points, on a temperature versus carbon concentration plot, where austenite and ferrite of the same chemical composition have the same free energy. T'_0 curve is defined similarly, but takes into account the stored energy of bainite transformation. When a bainite plate forms, the excess carbon immediately get distributed into the surrounding austenite, so the carbon concentration of untransformed austenite increases with the proceeding of transformation. Bainite transformation can occur if the carbon concentration of untransformed austenite is below that given by the T'_0 curve, so the maximum amount of bainite depends on the
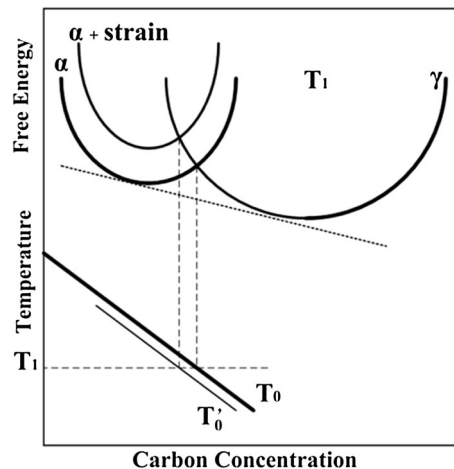
Fig. 14 Schematic illustration of the T_0 and T'_0 *curve* and the Gibbs free energy *curves* for ferrite and austenite at a temperature

maximum carbon content that can be stored in untransformed austenite. Larger ability of austenite to store carbon results in larger degree of bainitic transformation. Figure 14 shows that the maximum amount of carbon in the untransformed austenite increases with the decrease of temperature. It demonstrates that more bainite can be obtained at a lower transformation temperature. Therefore, the lengthening rate of bainite sheaves decreases while the amount of bainite increases with the decrease of temperature. The higher lengthening rate of bainite sheaves does not mean more amount of final bainite.

The main novelty of this work is that, the evolution of bainite lengthening rate during continuous cooling process is investigated by the approach that combines LSCM and dilatometry. Most previous studies on bainite transformation by in situ observation focused on the isothermal transformation process and the evolution of bainite lengthening rate during continuous cooling process has rarely been reported. In most industrial cases, bainite transformation normally occurs during continuous cooling, so that the investigation of bainite lengthening during continuous cooling is meaningful. The result enriches the theoretical study of bainite transformation.

4 Conclusions

The lengthening process of bainite sheaves was dynamically observed on LSCM in a Fe–C–Mn–Si superbainitic steel during continuous cooling process. The lengthening rates of bainite sheaves in three temperature ranges were calculated. The results indicated that the lengthening rate of bainite sheaves decreased with the decrease of temperature. The lengthening rate in high temperature range is larger due to the easy carbon diffusion, high nucleation rate, smaller carbon content and less plastic deformation in untransformed austenite. In addition, the lengthening rate of bainite sheaves nucleated at grain boundary was larger than that of bainite sheaves nucleated within grains. Furthermore, the microstructures after different isothermal holding temperatures were analyzed. The higher lengthening rate of bainite sheaves did not mean more amount of final bainite. More and finer bainite platelets could be obtained at lower bainite transformation temperature.

References

1. Muddle B C, and Nie J F, *Scr Mater* **47** (2002) 187.
2. Gupta C, Dey G K, Chakravartty J K, Srivastav D, and Banerjee S, *Scr Mater* **53** (2005) 559.
3. Koo M, Xu P, Tomota Y, and Suzuki H, *Scr Mater* **61** (2009) 797.
4. Hu H J, Xu G, Wang L, Xue Z L, Zhang Y L, and Liu G H, *Mater Des* **84** (2015) 95.
5. Tian J Y, Xu G, Zhou M X, Hu H J, and Wan X L, *Metals* **7** (2017) 40.
6. Zhou M X, Xu G, Wang L, and Hu H J, *Trans Indian Inst Met* **69** (2016) 693.
7. Huang C J, Browne D J, and Mcfadden S, *Acta Mater* **54** (2006) 11.
8. Sajjadi S A, and Zebarjad S M, *J Mater Process Technol* **189** (2007) 107.
9. Xu G, Liu F, Wang L, and Hu H J, *Scr Mater* **68** (2013) 833.
10. Kolmskog P, Borgenstam A, Hillert M, Hedström P, Babu S S, and Terasaki H, *Metall Mater Trans A* **43** (2012) 4984.
11. Yada H, Enomoto M, and Sonoyama T, *ISIJ Int* **35** (1995) 976.
12. Ji Y P, Liu X H, Liu Z C, and Ren H P, *Trans Mater Heat Treat* **35** (2014) 28.
13. Zhang D, Terasaki H, and Komizo Y I, *J Alloys Compd* **484** (2009) 929.
14. Hu Z W, Xu G, Hu H J, Wang L, and Xue Z L, *Int J Miner Metal Mater* **21** (2014) 371.
15. Hu H J, Xu G, Zhang Y L, Xue Z L, and Zhou M X, *J Wuhan Univ Technol* **30** (2015) 818.
16. Lee Y K, *J Mater Sci Lett* **21** (2002) 1253.
17. Kung C Y, and Rayment J J, *Metall Mater Trans A* **13** (1982) 328.
18. Ko T, and Cottrell S A, *J Iron Steel Inst* **172** (1952) 307.
19. Cabus C, Réglé H, and Bacroix B, *Mater Charact* **58** (2007) 332.
20. Matsuda H, and Bhadeshia H K D H, *Proc R Soc Lond A Math* **56** (1990) 263.
21. Bohemen S M C V, *Metall Mater Trans A* **41** (2009) 285.
22. Kang M, Zhang M X, and Zhu M, *Acta Mater* **54** (2006) 2121.
23. Hillert M, *Metall Mater Trans A* **25** (1994) 1957.
24. Hillert M, *Metall Mater Trans A* **6** (1975) 5.
25. Christian J W, *Mater Today* **6** (1965) 53.
26. Luzginova N V, Zhao L, and Sietsma J, *Mater Sci Eng A* **481** (2008) 766.
27. Oztur B, Fearing V L, Ruth J A, and Simkovich G, *Solid State Ionics* **12** (1984) 145.
28. Quidort D, and Brechet Y J M, *Acta Mater* **49** (2001) 4161.
29. Hu H J, Zurob H S, Xu G, Embury D, and Purdy G R, *Mater Sci Eng A* **626** (2015) 34.
30. Caballero F G, Santofimia M J, Garcia-Mateo C, Chao J, and Andres C G D, *Mater Des* **30** (2009) 2077.
31. Bhadeshia H K D H, David A S, Vitek J M, and Reed R W, *Mater Sci Technol* **7** (1991) 686.
32. Lindström A, Austempered high silicon steel: investigation of wear resistance in a carbide free microstructure, Master thesis, Luleå Tekniska Universitet. Sweden (2006).